

Phase Structure of a 3D Nonlocal U(1) Gauge Theory: Deconfinement by Gapless Matter Fields

Gaku Arakawa and Ikuo Ichinose

Department of Applied Physics, Nagoya Institute of Technology, Nagoya, 466-8555 Japan

Tetsuo Matsui

Department of Physics, Kinki University, Higashi-Osaka, 577-8502 Japan

Kazuhiko Sakakibara

Department of Physics, Nara National College of Technology, Yamatokohriyama, 639-1080 Japan

Shunsuke Takashima

Department of Applied Physics, Nagoya Institute of Technology, Nagoya, 466-8555 Japan

Abstract

In this paper, we study a 3D compact U(1) lattice gauge theory with a variety of nonlocal interactions that simulates the effects of gapless/gapful matter fields. This theory is quite important to investigate the phase structures of QED_3 and strongly-correlated electron systems like the 2D quantum spin models, the fractional quantum Hall effect, the t-J model of high-temperature superconductivity. We restrict the nonlocal interactions among gauge variables only to those along the temporal direction and adjust their coupling constants optimally to simulate the isotropic nonlocal couplings of the original models. We perform numerical studies of the model to find that, for a certain class of power-decaying couplings, there appears a second-order phase transition to the deconfinement phase as the gauge coupling constant is decreased. On the other hand, for the exponentially-decaying coupling, there are no signals for second-order phase transition. These results indicate the possibility that introduction of sufficient number of massless matter fields destabilizes the permanent confinement in the 3D compact U(1) pure gauge theory due to instantons.

1 Introduction

Gauge theories and their associated concepts play important roles not only in elementary particle physics but also in condensed matter physics. For example, the conventional superconducting phase transition is characterized as a change of the gauge dynamics of the electromagnetic U(1) gauge

symmetry from the Coulomb phase to the Higgs phase. Also, for a variety of strongly-correlated electron systems, it has been recognized that their phase structures and the properties of low-energy excitations are naturally described by using the terminology of gauge theories[1]. More explicitly, as such low-energy “quasi-particles”, the composite fermions/bosons in the fractional quantum Hall states[2] and the holons and spinons in the t-J model of high- T_c cuprates[3] have been proposed. It was argued[4] that their unconventional properties like fractionality and their existence itself may be explained by a confinement-deconfinement phenomenon of the gauge dynamics of the effective gauge theories derived from the original models. This interesting idea is still controversial[5], but certainly warrants further investigation.

Including this point, most of the problems in gauge-theoretical studies on the strongly-correlated electron systems reduce to studying the phase structure of gauge theories coupled to *gapless* relativistic/nonrelativistic matters. In the elementary particle physics, it is generally believed that phase structures of gauge systems coupled to matter field are *not* easy to study analytically because introduction of matter fields results in the lack of simple order parameters such as Wilson loops for pure gauge systems[6]. Furthermore, inclusion of gapless fermions make numerical simulations a difficult task since one must face quite nonlocal interactions generated by integrating over fermion variables. Generally speaking, one can expect that couplings to gapless matter fields may change the universality class of the gauge system under consideration from that of the pure gauge model. A good example is the four-dimensional (4D) QCD coupled with light quarks in which the number of light quarks strongly influences its phase structure[7].

In this paper, we address this problem of gauge dynamics of coupled systems. Explicitly, we are interested in the U(1) lattice gauge theory (LGT) with gapless/gapful and relativistic/nonrelativistic matter fields in three dimensions (two spatial dimensions at zero temperature). This theory of course covers the important model QED₃[8]. It appears also as a main part of the effective gauge theory of the strongly-correlated electron systems mentioned above, and so plays an important role in studying these systems[4, 9]. In the ordinary 3D compact U(1) pure gauge system (i.e., without matter fields) with local interactions, it is established that only the confinement phase is realized because of instanton condensation[11]. For the case with additional massless (gapless) matter fields coupled to the U(1) gauge field, recent studies give controversial results on the possibility of a deconfinement phase; it is supported in Ref.[4, 12] whereas it is denied in Ref.[13].

Our approach to this problem is by (i) introducing an effective theory of the original theory and (ii) studying its phase structure numerically. As the effective theory we use a 3D U(1) pure LGT with nonlocal interactions among gauge variables. These nonlocal interactions are along the temporal direction and mimic the effect of matter fields. We consider exponentially-decaying interactions for

massive matter fields (i.e., fields with gaps) and power-decaying interactions for massless (gapless) fields. We shall see that certain cases of power-decaying interactions exhibit second-order phase transitions which separate the confinement phase and the deconfinement phase[10]. The existence of the deconfinement phase in the effective theory indicates that it is realized in the original model if the number of gapless matter fields is sufficiently large. This result is in agreement with the results of Ref.[4, 12].

The rest of the paper is organized as follows. In section 2, the effect of matter fields is explained in several aspects like the perturbation theory, the large- N analyses, and the strongly-correlated electron systems. The reader who is interested in the model itself may skip these examples and directly go to section 3, in which the original model and its effective nonlocal gauge model are explained. In section 4, the effective model is studied by the low and high-temperature expansions. The analytical expressions of the internal energy and the specific heat are in good agreement with the numerical calculations in the following sections. Section 5 is devoted for numerical calculations. We calculate the internal energy, specific heat, expectation values of Polyakov loops, Wilson loops, and density of instantons. All these quantities indicate a second-order confinement-deconfinement phase transition (CDPT) for the gauge models with sufficiently long-range correlations among the gauge variables. In section 6, we study tractable low-dimensional spin models, which are obtained by simple reduction of the gauge degrees of freedom in the nonlocal effective model. Then we obtain an intuitive picture of the CDPT of the present long-range U(1) gauge theories. Section 7 is devoted for conclusion.

2 Effect of Matter Fields on Gauge Dynamics

In this section 2.1-2.4, we first review the effect of matter fields upon the U(1) gauge dynamics in several aspects. The reader who is interested in the nonlocal gauge model itself may skip this section and directly go to Sect.3.

2.1 Matter fields in perturbation theory

One may generally expect that inclusion of massless matter fields to a system of gauge field may drastically change the gauge dynamics at long wavelengths. Let us first study this phenomenon when the gauge coupling constant e is small $e \ll 1$ by considering a gauge system defined in a 3D continuum spacetime and using perturbation theory.

For the case that *relativistic and massless* matter fields are coupled to a $U(1)$ gauge field $A_\mu(x)$ ($\mu = 0, 1, 2$), the one-loop radiative correction of matter fields generates the following nonlocal term in the effective action of $A_\mu(x)$;

$$\Delta A \propto e^2 \int d^3x \int d^3y \sum_{\mu, \nu} F_{\mu\nu}(x) \frac{1}{|x-y|^2} F_{\mu\nu}(y), \quad F_{\mu\nu} = \partial_\mu A_\nu - \partial_\nu A_\mu. \quad (2.1)$$

It is obvious that the above term strongly suppresses fluctuations of $A_\mu(x)$ at long distances due to the factor $|x-y|^{-2}$. [Here the massless relativistic field means that its *renormalized mass* is vanishing. If the matter fields are *massive* with a mass m , this factor is replaced by a short-range one, $\exp(-m|x-y|)|x-y|^{-2}$.] The conventional Maxwell term is obtained by the replacement $|x-y|^{-2} \rightarrow \delta(x-y)$, and therefore the nonlocal terms are leading at low energies and momenta if its effective coupling constant does not vanish at the infrared limit. Then the potential energy $V(r)$ between two charges separated by distance r changes drastically,

$$V(r) \propto \log r \rightarrow V(r) \propto \frac{1}{r}. \quad (2.2)$$

2.2 Instantons in compact $U(1)$ gauge theory

In the compact $U(1)$ gauge theory, topologically nontrivial excitations (e.g. instantons) of $A_\mu(x)$ appear whose effect at small e can be estimated by replacing the field strength $F_{\mu\nu}(x)$ in Eq.(2.1) by $F_{\mu\nu}(x) - 2\pi n_{\mu\nu}(x)$, where $n_{\mu\nu}$ is an integer field whose rotation measures the instanton number(density) $\rho(x) = \epsilon_{\mu\nu\lambda} \partial_\mu n_{\nu\lambda}(x)$.

In the gauge model with the usual Maxwell term, the potential energy between a pair of instantons at distance r is Coulombic, $V_{\text{ins}}(r) \sim 1/r$. However, the long-range action (2.1) modifies $V_{\text{ins}}(r)$ to a long-range one[12],

$$V_{\text{ins}}(r) \propto \frac{1}{r} \rightarrow V_{\text{ins}}(r) \propto \log r. \quad (2.3)$$

Recently, it was argued that a gas of charged particles with the long-range interaction like $\log r$ exhibits a phase transition between a dilute gas of dipoles and a plasma[14]. This result implies that instantons in the long-range gauge theories form dipole pairs and do not condense in the weak-coupling region. Since the confinement phase of gauge dynamics requires a condensation of isolated instantons (a plasma phase), this result leads to a deconfinement phase of gauge dynamics there.

2.3 The CP^{N-1} model and the large- N analysis

To investigate the nonperturbative effect of matter fields in another approach, let us study the CP^{N-1} model in a 3D continuum by using the $1/N$ expansion[15]. The action of the model is given

as

$$A_{\text{CP}} = \int d^3x \left[|D_\mu z|^2 + \sigma \left(|z|^2 - \frac{1}{f} \right) \right], \quad (2.4)$$

where $z_a(x)$ ($a = 1, 2, \dots, N$) is the CP^{N-1} field satisfying the local constraint,

$$\sum_{a=1}^N z_a^*(x) z_a(x) = \frac{1}{f} \text{ for each } x \quad (2.5)$$

via the Lagrange multiplier field $\sigma(x)$.

$$D_\mu z = (\partial_\mu + iA_\mu)z, \quad A_\mu = iz^\dagger \partial_\mu z, \quad (2.6)$$

are the covariant derivatives and the composite U(1) gauge field, respectively. The system has a local U(1) gauge symmetry under $z_a(x) \rightarrow z'_a(x) \exp(i\theta(x))z_a(x)$.

At large N , the $1/N$ expansion is reliable and predicts a critical coupling f_c in the model. For $f > f_c$, the model is in the disordered-confinement phase in which $\langle \sigma(x) \rangle \neq 0$ and the correlation functions of gauge-invariant composite fields $n_{ab}(x)$ behave as

$$n_{ab}(x) \equiv \bar{z}_a(x) z_b(x), \quad \langle n_{ab}(x) n_{ab}(y) \rangle \simeq \exp(-m|x-y|), \quad m \propto \langle \sigma(x) \rangle. \quad (2.7)$$

n_{ab} describe the massive low-energy excitations in this phase. On the other hand, for $f < f_c$, the model is in the ordered-Higgs phase in which $\langle \sigma(x) \rangle = 0$ and the CP^{N-1} field has a nonvanishing expectation value like $\langle z_N(x) \rangle = v_0 \neq 0$. As a result, the gauge field A_μ acquires a finite mass ($\propto v_0$) by the Anderson-Higgs mechanism. The low-energy excitations are gapless and described by $z_a(x)$ ($a \neq N$) fields.

Then it is quite interesting to see how the gauge field behaves just at the *critical point* $f = f_c$. In the leading order of the $1/N$ expansion, it is shown that all the components $z_a(x)$ ($a = 1, 2, \dots, N$) are massless and the gauge field A_μ acquires the nonlocal “kinetic term” of Eq.(2.1). This implies that, at the critical point, the nonperturbative fluctuations of the gauge field like instantons are suppressed, so the gauge dynamics at $f = f_c$ is in the *Coulomb phase* with the potential $V(r) \sim 1/r$.

Very recently, we numerically studied the 3D $\text{CP}^1 + \text{U}(1)$ LGT from the above point of view[16]. This model contains two parameters; the CP^1 coupling of the spin stiffness f and the gauge coupling e , where we treat the compact gauge field and the CP^1 field as independent fields. We found that there exists a critical line of second-order phase transition emanating from the critical point of the CP^1 model [O(3) spin model] ($f = f_c, e = \infty$) and terminating at the O(4) spin model at ($f = f'_c, e = 0$). We also measured the instanton density and gauge-invariant gauge-boson mass near the critical line. From these results, we concluded that the confinement phase is realized on the critical line. However, calculations of CP^{N-1} model with $N = 3, 4, 5$ suggest that the nonlocal

term (2.1) tends to dominate and suppress the topologically nontrivial configurations in the CP^N model as $N \rightarrow \text{large}$. We expect that there exists a *deconfinement phase transition* for $N_c < N$ as suggested by the large- N analysis in the continuum. In fact, we note that a similar phenomenon has been observed for lattice QCD in four dimensions. For a sufficient large number of light flavors $N_f > 7$, the model stays in the deconfinement phase even for vanishing bare gauge coupling[7].

Let us comment on the relation between the instanton approach of section 2.2 and the present large- N analysis. The CP^{N-1} model is known to contain instantons for any N . By using this model Jevicki [17] argued that these two approaches for evaluation of the partition function by (i) the saddle-point method in the large- N limit and (ii) the summation over all the instanton configurations are equivalent in the sense that (i) and (ii) correspond to different choices of contours in a complex integral.

2.4 Nonrelativistic fermions in strongly-correlated electron systems

In general, nonrelativistic fermions are distinguished from relativistic fermions by the following properties; (i) they propagate only in the positive direction of the imaginary time in path-integral formulation, and (ii) they form a Fermi surface (line). In strongly correlated electron systems, one faces nonrelativistic fermions not only in the original models but also in their effective gauge models. In studying the fractionalization phenomena of electrons like the charge-spin separation (CSS) in high-temperature superconductivity and the particle flux separation (PFS) in fractional quantum Hall systems, we regard an electron C_x (we suppress the spin index for simplicity) at the site x of a 2D spatial lattice as a composite of a fermion A_x and a boson B_x as

$$C_x = A_x^\dagger B_x. \quad (2.8)$$

To assure the correct physical space composed of C_x , one imposes the local constraint for the physical states $|\text{phys}\rangle$ as

$$(A_x^\dagger A_x + B_x^\dagger B_x - 1)|\text{phys}\rangle = 0 \text{ for each } x. \quad (2.9)$$

In fact from this constraint, the following physical states appear correctly,

$$\begin{aligned} |\text{no-electron}\rangle &= A_x^\dagger |0\rangle, \\ |\text{one-electron}\rangle &= B_x^\dagger |0\rangle, \end{aligned} \quad (2.10)$$

where $|0\rangle$ is the empty state; $A_x|0\rangle = B_x|0\rangle = 0$. Then the hopping term of electrons (e.g., the t -term of the t-J model) may be rewritten up to the remaining two-body interactions via a “decoupling” as

$$C_{x+i}^\dagger C_x + \text{H.c.} = B_{x+i}^\dagger A_{x+i} A_x^\dagger B_x + \text{H.c.}$$

$$\Rightarrow B_{x+i}^\dagger V_{xi} B_x + A_{x+i}^\dagger V_{xi}^\dagger A_x + \text{H.c} - |V_{xi}|^2. \quad (2.11)$$

V_{xi} is an auxiliary complex field defined on the link $(x, x + \hat{i})$ where $i = 1, 2$ is the direction index of the lattice. Its phase degree of freedom $U_{xi} \equiv V_{xi}/|V_{xi}|$ behaves as a *spatial component* of a compact U(1) gauge field $U_{xi} [= \exp(i\theta_{xi})]$. U_{xi} represents the binding force of the constituents A_x and B_x . In the path-integral formalism, the partition function $\text{Tr}_C \equiv \exp[-\beta H(C)]$ ($\beta \equiv T^{-1}$) has the following representation:

$$\begin{aligned} Z &= \int \prod_{x,\tau} d\bar{A}_x(\tau) dA_x(\tau) dB_x(\tau) \prod_{\mu=0,1,2} dU_{x\mu}(\tau) \exp(A), \\ A &= \int_0^\beta d\tau \sum_x \left[-i\theta_{x0} - \bar{A}_x(\partial_0 - i\theta_{x0} + \mu_A) A_x - \bar{B}_x(\partial_0 - i\theta_{x0} + \mu_B) B_x \right. \\ &\quad \left. + t \sum_i (\bar{A}_{x+i} U_{xi}(\tau) B_x + \text{H.c.}) + A_{\text{int}} \right], \end{aligned} \quad (2.12)$$

where τ ($\in [0, \beta]$) is the continuum imaginary time, $A_x(\tau)$ is a Grassmann number expressing fermions, $\mu_{A(B)}$ is the chemical potential, and t is the hopping amplitude. The field θ_{x0} is a Lagrange multiplier field to enforce the constraint (2.9). It may be viewed as the time-component of gauge field. In fact, in the discrete-time formulation on the 3D lattice it appears as the exponent of gauge variable in the τ -direction, $U_{x0} = \exp(i\theta_{x0})$.

The gauge dynamics of $U_{x\mu}$ is generally classified into two categories; (i) the deconfinement phase in which fluctuations of the phases $\theta_{x\mu}$ are (around certain pure gauge configuration, say $\theta_{x\mu} = 0$) are small, and (ii) the confinement phase in which $\theta_{x\mu}$ fluctuate wildly. The deconfinement phase is further classified according to the mass m of $\theta_{x\mu}$; $m = 0$ in the Coulomb phase and $m \neq 0$ in the Higgs phase. As mentioned, U_{xi} express the binding force among A_x and B_x . When the gauge dynamics of U_{xi} is realized in the confinement phase, these constituents are bound within electrons and the relevant low-energy quasi-particles are described by the electron operators C_x themselves. On the other hand, if the gauge dynamics is realized in the deconfinement phase, the binding force is weak and these constituents are no more bound in each electron but dissociate each other. This is just the the fractionalization(separation) phenomena of electrons. The low-energy quasi-particles of the system are then described by the asymptotic fields of A_x and B_x .

In Ref.[4] we have studied the system of Eq.(2.12) at finite temperatures (T) by the hopping expansion in the temporal gauge $\theta_{x0} = 0$. After integrating over A_x and B_x in powers of t , one obtains the effective interactions. Up to $O(t^2)$, by restoring the temporal components U_{x0} , one gets the following effective interaction among $U_{x\mu}$,

$$\Delta A \propto \delta(1 - \delta) \cdot t^2 \sum_{x,i} \int_0^\beta d\tau \int_0^\beta d\tau' \bar{V}_{x\perp,i}(\tau, \tau') V_{x\perp,i}(\tau, \tau'),$$

$$V_{x_\perp, i}(\tau, \tau') \equiv \bar{U}_{x_\perp, \tau', i} \exp \left(i \int_\tau^{\tau'} d\tau'' [\theta_{x_\perp + \hat{i}, 0}(\tau'') - \theta_{x_\perp, 0}(\tau'')] \right) U_{x_\perp, \tau, i}, \quad (2.13)$$

where $\delta = \langle A_x^\dagger A_x \rangle$ is the concentration of fermions. The corresponding terms are illustrated in Fig.1.

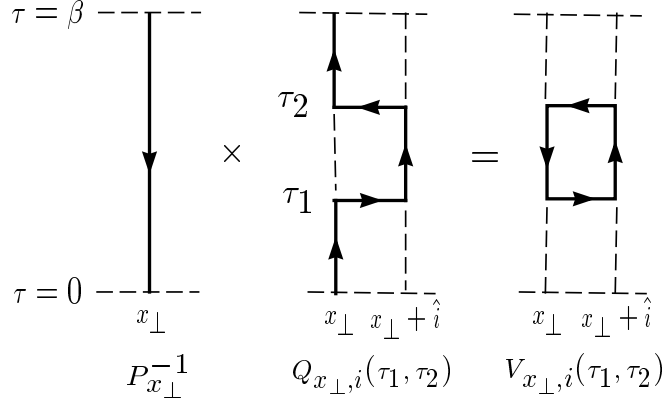


Figure 1: Illustration of the nonlocal interactions in electron-fractionalization phenomena. $P_{x_\perp} = \exp(i \int d\tau \theta_{x_0})$ is the Polyakov line at the transverse coordinate $x_\perp = (x_1, x_2)$, $Q_{x_\perp, i}(\tau_1, \tau_2)$ is given by product of propagators $\langle B_{x_\perp}(\tau_1) B_{x_\perp}^\dagger(\tau_2) \rangle$ and $\langle A_{x_\perp}(\tau_2) A_{x_\perp}^\dagger(\tau_1) \rangle$. The product of these terms results an effective interaction $V_{x_\perp, i}(\tau_2, \tau_1)$ along a closed loop, which has the same form as a vacuum polarization of relativistic matter fields.

The interactions among $U_{x\mu}(\tau)$ in ΔA are quite nonlocal in the τ -direction, and ΔA favors the ordered configurations of $U_{x\mu}$, so the deconfinement phase. In the previous papers[4], we argued that this is the essence of the mechanism of fractionalization phenomena like CSS and PFS. By mapping these gauge models approximately to a spin model, we concluded that the U(1) gauge dynamics is realized in the deconfinement phase at the low- T region *below* certain critical line $T_c(\delta)$. Thus the possible deconfinement phase in the model similar to Eq.(2.13) is to support the electron fractionalization phenomena.

3 Nonlocal Lattice Gauge Theory

In the previous section, we have seen various approaches to study the effect of matter fields upon U(1) gauge dynamics. To confirm these results, one must examine the validity of the approximations employed there. In particular, to check the validity of the hopping expansion at $T = 0$ explained in Sect.2.4 is quite important to understand the basic properties of strongly-correlated electron systems.

Keeping this problem in mind, we start this section with a U(1) LGT coupled with matter fields and introduce its effective nonlocal LGT. Let us consider a 3D cubic lattice with a discrete imaginary time instead of the continuous imaginary time. The gauge field $U_{x\mu}$ ($\mu = 0, 1, 2$) is defined on the link $(x, x + \hat{\mu})$ between the pair of nearest-neighbor sites x and $x + \hat{\mu}$. The partition function Z is given by the following functional integral,

$$\begin{aligned} Z &= \int \prod_x d\bar{\phi}_x d\phi_x \prod_{x\mu} dU_{x\mu} \exp(A), \\ A &= - \sum_{x,y} \bar{\phi}_x \Gamma_{xy}(U) \phi_y + A_U, \\ A_U &= q \sum_{x,\mu < \nu} (\bar{U}_{x\mu} \bar{U}_{x+\hat{\mu},\mu} U_{x+\hat{\mu},\nu} U_{x\mu} + c.c.), \end{aligned} \quad (3.14)$$

where $x = (x_0, x_1, x_2)$ is the site-index of the 3D lattice of the size $V = N_0 N_1 N_2$ with the periodic boundary condition, $\mu (= 0, 1, 2)$ is the (imaginary) time and spatial direction index, ϕ_x is the matter field on x , $U_{x\mu} = \exp(i\theta_{x\mu})$ ($-\pi < \theta_{x\mu} \leq \pi$) is the $U(1)$ gauge variable on the link $(x, x + \hat{\mu})$, and q is inverse gauge coupling constant. $\Gamma_{xy}(U)$ represents the *local* minimal couplings of ϕ_x to $U_{x\mu}$. For example, for a bosonic matter field whose quantum carries charge Q , one has

$$\sum_{x,y} \bar{\phi}_x \Gamma_{xy}(U) \phi_y = t \sum_{x,\mu} \left[\bar{\phi}_{x+\hat{\mu}} (U_{x\mu})^Q \phi_x + \text{H.c.} \right] + M^2 \sum_x \bar{\phi}_x \phi_x, \quad M^2 = 6 + m^2, \quad (3.15)$$

where m^2 is the mass in unit of the lattice spacing and 6 in M^2 is the number of links emanating from each site. In the rest of discussion, we consider the case of $Q = 1$ for simplicity.

After integrating over the matter field ϕ_x , effective gauge model is obtained, which includes all contributions from ϕ_x to the gauge dynamics,

$$Z = \int \prod_{x\mu} dU_{x\mu} \exp \left[f \text{Tr} \log \Gamma_{xy}(U) + A_U \right], \quad (3.16)$$

where f is a parameter counting the statistics and internal degrees of freedom of ϕ_x . Due to the $(\text{Tr} \log \Gamma_{xy}(U))$ term, the effective gauge theory becomes *nolocal*. For relativistic matter fields, a formal expression of the effective gauge theory action is obtained by the hopping expansion and it is expanded as a sum over all the closed random walks \mathcal{R} (loops including backtrackings) on the 3D lattice, which represent world lines of particles and antiparticles as

$$\text{Tr} \log \Gamma_{xy}(U) = \sum_{\mathcal{R}} \frac{\gamma^{L[\mathcal{R}]} }{L[\mathcal{R}]} \prod_{(x\mu) \in \mathcal{R}} U_{x\mu}. \quad (3.17)$$

$L[\mathcal{R}]$ is the length of \mathcal{R} , and $\gamma = (6 + m^2)^{-1}$ is the hopping parameter. There are many different random walks that have the same shape of a closed loop on the lattice. Each random walk in such a family may have a different starting point and/or backtrackings. This degeneracy cancels out the

denominator $L[\mathcal{R}]$ in Eq.(3.17). For the constant gauge-field configuration $U_{x\mu} = 1$, the expansion in (3.17) is logarithmically divergent $\sim \log m$ as $m \rightarrow 0$ due to the lowest-energy zero-momentum mode.

Below we shall study a slightly more tractable model than that given by Eq.(3.16). It is suggested by the formal hopping expansion (3.17), and obtained by retaining only the rectangular loops extending in the τ -direction in the loop sum and choosing their expansion coefficients as follows;

$$\begin{aligned}
Z_\tau &= \int \prod_{x\mu} dU_{x\mu} \exp(A_\tau), \\
A_\tau &= g \sum_x \sum_{i=1}^2 \sum_{\tau=1}^{N_0} c_\tau (V_{x,i,\tau} + \bar{V}_{x,i,\tau}) + A_S, \\
V_{x,i,\tau} &= \bar{U}_{x+\hat{\tau}\hat{0},i} \prod_{k=0}^{\tau-1} [\bar{U}_{x+k\hat{0},0} U_{x+\hat{i}+k\hat{0},0}] U_{xi}, \\
A_S &= g\lambda \sum_x (\bar{U}_{x2} \bar{U}_{x+\hat{2},1} U_{x+\hat{1},2} U_{x1} + \text{c.c.}),
\end{aligned} \tag{3.18}$$

where g is the (inverse) gauge coupling constant, and $V_{x,i,\tau}$ is the product of $U_{x\mu}$ along the rectangular $(x, x + \hat{i}, x + \hat{i} + \tau\hat{0}, x + \tau\hat{0})$ of size $(1 \times \tau)$ in the $(i - 0)$ plane. See Fig.2.

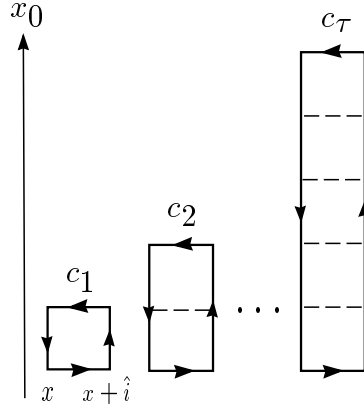


Figure 2: Illustration of the nonlocal interaction in the action (3.18). Each rectangle with thick lines represents $V_{x,i,\tau}$.

In A_S , we have retained only the single-plaquette coupling with the coefficient $(g\lambda)$. For the nonlocal coupling constant c_τ , we consider the following three cases;

$$c_\tau = \begin{cases} \tau^{-\alpha}, & \text{power - law decay (PD-}\alpha\text{)} (\alpha = 1, 2, 3), \\ e^{-m\tau}, & \text{exponential decay (ED),} \\ 1, & \text{no decay (ND).} \end{cases} \tag{3.19}$$

The power $\alpha = 1$ in the PD model in (3.19) reflects the effect of the *relativistic* massless excitations without dimensional parameters. In fact, this c_τ generates a logarithmically divergent action for $U_{x\mu} = 1$ explained below Eq.(3.17) as one can see from the relation, $\sum_\tau \exp(-m\tau)\tau^{-1} \simeq \log(1/m)$. The action for $m = 0$ is then proportional to $\sum_\tau \tau^{-1} \simeq \log N_0$ for finite N_0 . On the other hand, the ED model contains the parameter m with mass dimension and simulates the case of massive matter fields. (We used Eq.(3.19) instead of $\exp(-m\tau)/\tau$ to make the comparison with the PD case more definitive.) The ND model corresponds to gauge model coupled to *nonrelativistic* fermions with a Fermi surface (or Fermi line) as it is seen from Eq.(2.13).

4 High- and Low-Temperature Expansions

In this section we study the behavior of the models in two parameter regions of g by analytic methods; the region of small $g (<< 1)$ by high-temperature expansion (HTE) and the region of large $g (>> 1)$ by low-temperature expansion (LTE). Once one obtains an approximate expression for the partition function $Z_\mathcal{T}$, one can calculate various thermodynamic quantities. In particular, we are interested in the following “internal energy” E and the “specific heat” C of the model;

$$\begin{aligned} E &\equiv -\frac{1}{V}\langle A_\mathcal{T} \rangle = -\frac{1}{V} \frac{g}{Z_\mathcal{T}} \frac{dZ_\mathcal{T}}{dg} = g \frac{dF}{dg}, \\ C &\equiv \frac{1}{V}\langle (A_\mathcal{T} - \langle A_\mathcal{T} \rangle)^2 \rangle = -g^2 \frac{d^2 F}{dg^2}. \end{aligned} \quad (4.20)$$

We shall see that the results of the present section are in agreement with the numerical calculations of the following section.

Here we note that the above definition of C is the response of E under the variation of g and is different from the conventional specific heat that measures the response under the variation of temperature itself. The latter contains extra terms associated with the change of N_0 . Because these terms behave less singular than the variance of E , they are irrelevant in searching for phase transitions.

4.1 High-Temperature Expansion (HTE) for small g

Let us consider the case of small g . Since the action $A_\mathcal{T}$ is proportional to g , one may expand the partition function $Z_\mathcal{T}$ of (3.18) in powers of g as

$$Z_\mathcal{T} = \int [dU] \sum_{n=0}^{\infty} \frac{(A_\mathcal{T})^n}{n!}. \quad (4.21)$$

We obtain the expansion up to $O(g^4)$ as

$$Z_T = 1 + (B_{2T} + B_{2S}\lambda^2)g^2 + B_{3T}g^3 + (B_{4T} + B_{4TS}\lambda^2 + B_{4S}\lambda^4)g^4 + O(g^6), \quad (4.22)$$

where each coefficient is expressed as

$$\begin{aligned} B_{nT} &= \frac{1}{n!} \int [dU] \left[\sum_q c_\tau (V_q + \bar{V}_q) \right]^n, \quad q \equiv (x, i, \tau), \\ B_{nS} &= \frac{1}{n!} \int [dU] \left[\sum_p (U_p + \bar{U}_p) \right]^n, \quad U_p \equiv \bar{U}_{x+2,1} U_{x+1,2} U_{x1} \bar{U}_{x2}, \\ B_{4TS} &= \frac{4C_2}{4!} \int [dU] \left[\sum_p (U_p + \bar{U}_p) \cdot \sum_q c_\tau (V_q + \bar{V}_q) \right]^2. \end{aligned} \quad (4.23)$$

To evaluate the above coefficients, we use the following formula for U(1) integral,

$$\int dU_{x\mu} \bar{U}_{x\mu}^m U_{y\nu}^n = \delta_{xy} \delta_{\mu\nu} \delta_{mn}. \quad (4.24)$$

Then we obtain the following result;

$$\begin{aligned} B_{2T} &= \sum_q c_\tau^2 = 2VQ_2, \quad Q_2 \equiv \sum_\tau c_\tau^2, \\ B_{2S} &= \sum_p 1 = V, \\ B_{3T} &= \frac{3 \cdot 2}{3!} \sum_x \sum_i \sum_{\tau_1} \sum_{\tau_2} c_{\tau_1} c_{\tau_2} c_{\tau_3} V_{x,i,\tau_1} V_{x+\tau_1 \hat{0}, i, \tau_2} \bar{V}_{x,i,\tau_3} \delta_{\tau_3, \tau_1 + \tau_2} + \text{c.c.} \\ &= 4V\tilde{Q}_3, \quad \tilde{Q}_3 \equiv \sum_{\tau_1=1}^N \sum_{\tau_2=1}^N \sum_{\tau_3=1}^N c_{\tau_1} c_{\tau_2} c_{\tau_3} \delta_{\tau_3, \tau_1 + \tau_2}, \\ B_{4T} &= B_{4T}^a + B_{4T}^b + B_{4T}^c, \\ B_{4T}^a &= \frac{1}{4!} \sum_{q_1, q_2, q_3, q_4} \prod_{\ell=1}^4 c_{\tau_\ell} \cdot 4C_2 [\delta_{q_1 q_2} \delta_{q_3 q_4} + \delta_{q_1 q_3} \delta_{q_2 q_4} - \delta_{q_1 q_2} \delta_{q_2 q_3} \delta_{q_3 q_4}] \\ &= 2V^2 Q_2^2 - \frac{1}{2} V Q_4, \quad Q_4 \equiv \sum_\tau c_\tau^4, \\ B_{4T}^b &= \frac{4 \cdot 3 \cdot 2}{4!} \sum_{x,i} \sum_{\tau_1, \tau_2, \tau_3, \tau_4} c_{\tau_1} c_{\tau_2} c_{\tau_3} c_{\tau_4} (1 - \delta_{\tau_1 \tau_3}) \delta_{\tau_4, \tau_1 + \tau_2 - \tau_3} V_{x,i,\tau_1} V_{x+\tau_1 \hat{0}, i, \tau_2} \bar{V}_{x,i,\tau_3} \bar{V}_{x+\tau_3 \hat{0}, i, \tau_4} \\ &= 2V(\tilde{Q}_{4-} - Q_2^2), \quad \tilde{Q}_{4-} \equiv \sum_{\tau_1, \tau_2, \tau_3, \tau_4} c_{\tau_1} c_{\tau_2} c_{\tau_3} c_{\tau_4} \delta_{\tau_4, \tau_1 + \tau_2 - \tau_3}, \\ B_{4T}^c &= \frac{4!}{4!} \sum_{x,i} \sum_{\tau_1, \tau_2, \tau_3, \tau_4} c_{\tau_1} c_{\tau_2} c_{\tau_3} c_{\tau_4} V_{x,i,\tau_1} V_{x+\tau_1 \hat{0}, i, \tau_2} V_{x+(\tau_1 + \tau_2) \hat{0}, i, \tau_3} \bar{V}_{x,i,\tau_4} \delta_{\tau_4, \tau_1 + \tau_2 + \tau_3} + \text{c.c.} \\ &= 4V\tilde{Q}_{4+}, \quad \tilde{Q}_{4+} \equiv \sum_{\tau_1, \tau_2, \tau_3, \tau_4} c_{\tau_1} c_{\tau_2} c_{\tau_3} c_{\tau_4} \delta_{\tau_4, \tau_1 + \tau_2 + \tau_3}, \\ B_{4TS} &= \frac{1}{4} \sum_p 2 \cdot \sum_q 2c_\tau^2 = 2V^2 Q_2, \end{aligned}$$

$$\begin{aligned}
B_{4S} &= \frac{1}{4!} \sum_{p_1, p_2, p_3, p_4} {}_4C_2 [\delta_{p_1 p_2} \delta_{p_3 p_4} + \delta_{p_1 p_3} \delta_{p_2 p_4} - \delta_{p_1 p_2} \delta_{p_2 p_3} \delta_{p_3 p_4}] \\
&= \frac{1}{2} V^2 - \frac{1}{4} V.
\end{aligned} \tag{4.25}$$

Some of them are illustrated in Fig.3.

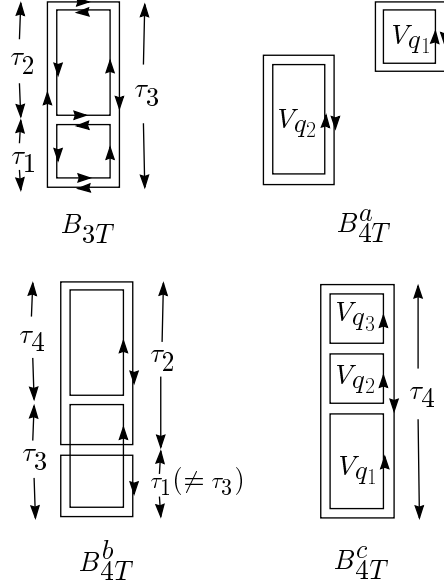


Figure 3: Illustration of the terms (4.25) in HTE. Each rectangle represents $V_{x,i,\tau}$. The terms $B_{3T}, B_{4T}^{b,c}$ reflect the nonlocal nature; they are absent in models of local interaction characterized by $c_\tau = 0(\tau > 1)$.

Finally, we obtain the expression of the partition function and the free energy as follows,

$$\begin{aligned}
Z_T &= \exp(-FV), \\
F &= -(2Q_2 + \lambda^2)g^2 - 4\tilde{Q}_3g^3 + \left(\frac{Q_4}{2} + \frac{\lambda^4}{4} - 4\tilde{Q}_{4+} - 2\tilde{Q}_{4-}\right)g^4 + O(g^6).
\end{aligned} \tag{4.26}$$

In the following, we list up the values of Q_2 and Q_4 for $N \rightarrow \infty$,

	Q_2	Q_4	
PD-1	$\frac{\pi^2}{6} = 1.64493$	$\frac{\pi^4}{90} = 1.08232$	
PD-2	$\frac{\pi^4}{90}$	$\frac{\pi^8}{9450} = 1.00408$	
PD-3	$\frac{\pi^6}{945} = 1.01734$	1.00025	
ED	0.15652	0.018657	

(4.27)

By using the approximate partition function $Z_{\mathcal{T}}$ of Eq.(4.26), we obtain

$$\begin{aligned} E &= -2(2Q_2 + \lambda^2)g^2 - 12\tilde{Q}_3g^3 + 4\left(\frac{Q_4}{2} + \frac{\lambda^4}{4} - 4\tilde{Q}_{4+} - 2\tilde{Q}_{4-}\right)g^4 + O(g^6), \\ C &= 2(2Q_2 + \lambda^2)g^2 + 24\tilde{Q}_3g^3 - 12\left(\frac{Q_4}{2} + \frac{\lambda^4}{4} - 4\tilde{Q}_{4+} - 2\tilde{Q}_{4-}\right)g^4 + O(g^6). \end{aligned} \quad (4.28)$$

Although the details of the numerical simulations will be given in the next section, let us compare here (4.26) and the MC result.

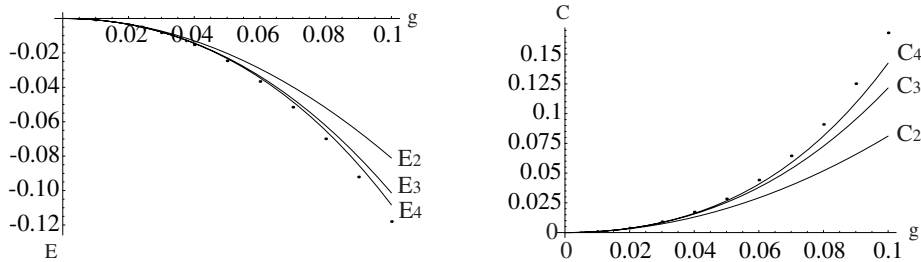


Figure 4: Comparison of HTE and the MC simulation. We compare the HTE results and the MC results of E and C for the PD-1 model with $N = 8$ and $\lambda = 1$. The curves indicated by E_n and C_n are the HTE results with the terms up to $O(g^n)$. The dots are the MC data.

Fig.4 shows that, as one includes the higher-order terms, the HTE results approaches the MC result systematically. However, the approach is rather slow compared with the related models of local interactions like the 3D XY spin model or the 3D U(1) pure LGT. This is because the present nonlocal interactions generate various important higher-order terms in the HTE that are absent from the local models.

Let us comment on the convergence of the HTE. As usual, the HTE is an expansion in the disordered (confinement) phase in which $U_{x\mu}$ fluctuates wildly. Equation (4.26) shows that the convergence radius g_{HTE} of the expansion is finite $g_{\text{HTE}} \neq 0$, because both the harmonic numbers Q_2 and Q_4 appearing in the coefficients are finite. This means that there exists certainly the finite region $0 \leq g^2 < g_{\text{HTE}}^2$ of the confinement phase. We notice that if the long-range interaction c_{τ} is very strong such that $Q_2 = \infty$, the confinement phase may disappear.

4.2 Low-Temperature Expansion (LTE) for large g

For large g , we evaluate $Z_{\mathcal{T}}$ by the LTE. The LTE is an expansion in powers of g^{-1} around a fixed “lowest-energy configuration” of $U_{x\mu}$ like $U_{x\mu} = 1$, which gives rise to the global maximum of $A_{\mathcal{T}}$.

Let us expand $U_{x\mu}$ as

$$U_{x\mu} \equiv \exp(i\theta_{x\mu}) = 1 + i\theta_{x\mu} - \frac{1}{2}\theta_{x\mu}^2 + O(\theta_{x\mu}^3), \quad (4.29)$$

where $\theta_{x\mu}$ is treated as $O(g^{-1/2})$ as we shall see. $A_{\mathcal{T}}$ is expanded up to the second order in $\theta_{x\mu}$ in the following quadratic form;

$$A_{\mathcal{T}} = 4gQ_1V + 2g\lambda V - g \sum_{x,\mu} \sum_{y,\nu} \theta_{x\mu} G_{x\mu,y\nu}(\lambda) \theta_{y\nu} + O(\theta^4), \quad (4.30)$$

where the first two terms $4gQ_1V + 2g\lambda V$ come from the first term, unity, of R.H.S. of Eq.(4.29). Due to the gauge invariance, one may extend the region of $\theta_{x\mu}$ from $\theta_{x\mu} \in (-\pi, \pi)$ to $\theta_{x\mu} \in (-\infty, \infty)$ together with a gauge fixing. We take the temporal gauge $\theta_{x0} = 0$ in the following calculation. Then we evaluate $Z_{\mathcal{T}}$ by rescaling $\theta'_{xi} = g^{1/2}\theta_{xi}$ and performing Gaussian integration as

$$\begin{aligned} Z_{\mathcal{T}} &\simeq e^{(4Q_1+2\lambda)gV} \prod_x \left[\int_{-\infty}^{\infty} d\theta_{x1} \int_{-\infty}^{\infty} d\theta_{x2} \right] \exp \left(-g \sum_{x,\mu} \sum_{y,\nu} \theta_{x\mu} G_{x\mu,y\nu} \theta_{y\nu} \right) \\ &= e^{(4Q_1+2\lambda)gV} \prod_x \left[g^{-1} \int_{-\infty}^{\infty} d\theta'_{x1} \int_{-\infty}^{\infty} d\theta'_{x2} \right] \exp \left(- \sum_{x,\mu} \sum_{y,\nu} \theta'_{x\mu} G_{x\mu,y\nu} \theta'_{y\nu} \right) \\ &= \exp \left[(4Q_1g + 2\lambda g - \ln g)V - \frac{1}{2} \text{Tr} \ln G(\lambda) \right], \\ F &= -(4Q_1 + 2\lambda)g + \ln g + O(g^0). \end{aligned} \quad (4.31)$$

This gives

$$\begin{aligned} E &= -(4Q_1 + 2\lambda)g + 1 + O(g^{-1}), \\ C &= 1 + O(g^{-1}). \end{aligned} \quad (4.32)$$

The higher-order terms in F are $O(g^{-n})$ ($n \geq 0$) which may be calculated by the usual perturbation theory. We shall see in the next section that the MC results approach the result of LTE of (4.32) at large g 's.

5 Numerical Results

In this section, we report our numerical calculations of the internal energy, the specific heat, the Polyakov lines, etc., and determine the phase structure of the models. Most of our interest concerns a possible CDPT in the 3D compact U(1) gauge models with the nonlocal interactions.

In the MC simulations, we consider the isotropic lattice, $N_{\mu} = N$ ($\mu = 0, 1, 2$), with the periodic boundary condition up to $N = 32$, where the limit $N \rightarrow \infty$ corresponds to the system on a 2D spatial lattice at $T = 0$. For the mass of the ED model, we set $m = 1$. For the spatial coupling λ scaled by g , we consider the two typical cases $\lambda = 0$ (i.e., no spatial coupling) and $\lambda = 1$.

5.1 Internal energy and specific heat

First we consider the PD-1 and ED models and calculate the “internal energy” E and the “specific heat” C of Eq.(4.20) in these systems.

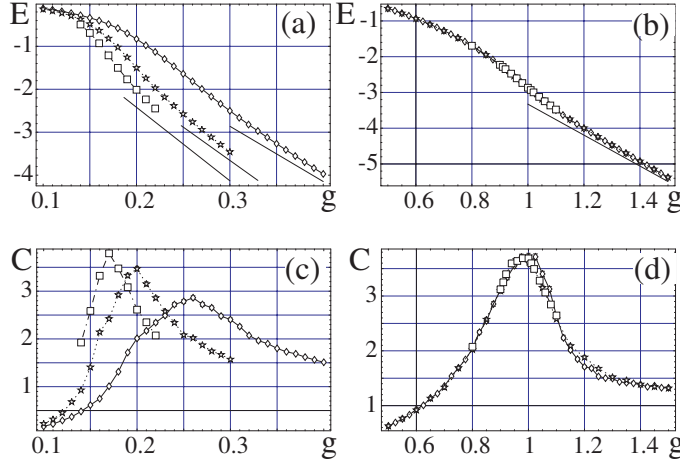


Figure 5: Internal energy E and its fluctuation C of the action with $\lambda = 1$ vs non-local coupling g for $N = 8(\blacklozenge), 16(\star), 24(\blacksquare)$; (a,c) PD-1 model, (b,d) ED model. The solid lines in (a) and (b) are the large- g expansion. In the PD-1 model, strong N dependence is observed in E at large g and in the developing peak of C . They indicate a second-order phase transition in the PD-1 model. In the ED model, on the other hand, C does not develop and therefore the observed peak indicates not a phase transition but a crossover.

In Fig.5, we present E and C for $\lambda = 1$ vs the nonlocal coupling g . They are consistent with the previous calculations of the HTE and LTE. In the PD-1 model ($\alpha = 1$), E of Fig.5(a) connects the HTE result and LTE result. Since the LTE is an expansion around $V_{x,i,\tau} = 1$, this behavior implies $V_{x,i,\tau} \sim 1$ for large g . C in Fig.5(c) shows that its peak develops as the system size N increases. These two points indicate that the PD-1 model exhibits *a second-order phase transition separating the disordered (confinement) phase and the ordered (deconfinement) phase* at $g = g_c \simeq 0.17$ which is determined from the data of $N = 24$. The existence and the nature of the phase transition will be confirmed later by the measurement of the Polyakov lines and the instanton density as we show in the following subsections.

We notice that the location of the peak in C of Fig.5(c) shifts to *smaller* g as the system size N increases in the direction opposite to the usual second-order phase transitions. This behavior reflects the fact that the couplings among $U_{x\mu}$ increases effectively as N increases due to the additional

terms in the summation over N_0 in the action even if one fixes the overall constant g . This is the characteristic nature of nonlocal interactions in strong contrast to local interactions.

On the contrary, in the ED model of Fig.5(d), the peak of C does not develop as N increases, showing *no* signals of a second-order transition. It may have a higher-order transition or just a *crossover*. Similar behavior of C is observed in the ordinary U(1) gauge systems with local actions which have only the confinement phase. The physical meaning of the above “crossover” in the ED model shall become clear by studying instantons in Sect.5.3.

It is quite interesting to see whether the data of C for $N = 8, 16$ and 24 in Fig.5(c) exhibit the finite-size scaling behavior[18]. To this end, let us introduce a parameter

$$\epsilon \equiv (g - g_\infty)/g_\infty \quad (5.33)$$

where g_∞ is the critical gauge coupling of the infinite system at $N \rightarrow \infty$. Then let us assume that the correlation length ξ scales as $\xi \propto \epsilon^{-\nu}$ with a critical exponent ν . We also expect that the peak of C diverges as $C_{\text{peak}} \propto \epsilon^{-\sigma}$ as $N \rightarrow \infty$ with another critical exponent σ . The finite-size scaling hypothesis predicts that the specific heat $C(\epsilon, N)$ for sufficiently large N scales as

$$C(\epsilon, N) = N^{\sigma/\nu} \phi(N^{1/\nu} \epsilon), \quad (5.34)$$

where $\phi(x)$ is a certain scaling function. In Fig.6, we present $\phi(x)$ determined by using the data in Fig.5(c) with $\nu = 1.2$, $\sigma/\nu = 0.25$ and $g_\infty = 0.11$. This result indicates that the finite-size scaling law holds quite well. Considering the errors in the data we estimate the values of scaling parameters and g_∞ as

$$\nu = 1.2 \sim 1.3, \sigma/\nu = 0.25 \sim 0.26, g_\infty = 0.10 \sim 0.12. \quad (5.35)$$

The simulations of the PD-1 and ED models with $\lambda = 0$ give similar behaviors of E and C as the $\lambda = 1$ case, preserving the above phase structure for $\lambda = 1$. That is, the PD-1 model ($\lambda = 0$) has a CDPT, while the ED model ($\lambda = 0$) has no transition.

Let us next consider the ND model. In Fig.7, we present C for $\lambda = 0$ and 1 , which show strong signals of a second-order phase transition. However, the value of the critical coupling for $\lambda = 1$, $g_c \sim 0.1(N = 8), 0.045(N = 16), 0.03(N = 24)$, decreases very rapidly as the system size increases. This behavior is explained by the increase of effective coupling explained above. Then one may think that $g_c \rightarrow 0$ as $N \rightarrow \infty$, i.e., only the deconfinement phase survives in the ND model. This expectation is consistent with the fact that the coefficient of the HTE for small g , $Q_2 = \sum_\tau c_\tau^2$ diverges as $Q_2 \propto N^2 \rightarrow \infty$ for the ND model, i.e., the radius of convergence in the HTE is zero. On the contrary, Q_2 is finite for the PD-1 model, assuring us $g_c \neq 0$. This is supported also by the scaling analysis given above.

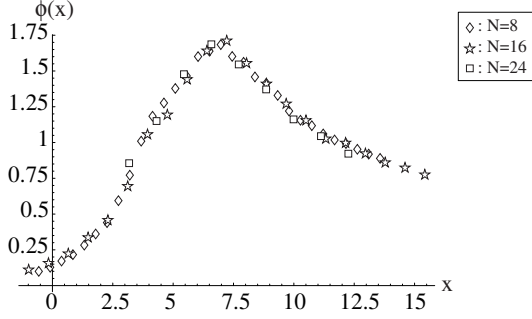


Figure 6: Scaling function $\phi(x)$ of (5.34) obtained from the data C of the PD-1 model in Fig.5(c) for $N = 8, 16$ and 24 . The result obviously shows that the finite-size scaling law holds and the observed phase transition in the PD-1 model is of second-order.

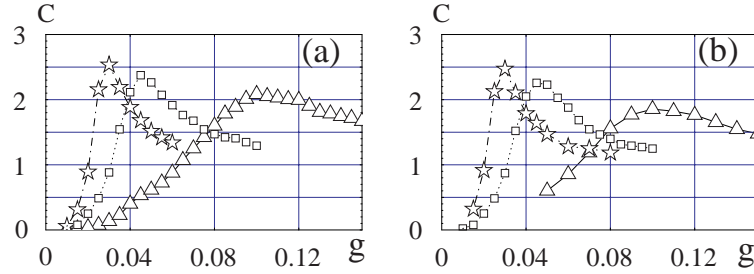


Figure 7: C vs g in the ND model with (a) $\lambda = 0$ and (b) $\lambda = 1$ for $N = 8(\blacktriangle), 16(\blacksquare), 24(\star)$. The peaks develops as the system-size increases.

From these results for the various cases of long-range interaction, it seems that there exists a *critical power* $\alpha = \alpha_c$ below which the CDPT takes place. In Fig.8 we show C of the PD model with $\alpha = 2$ and $\alpha = 3$.

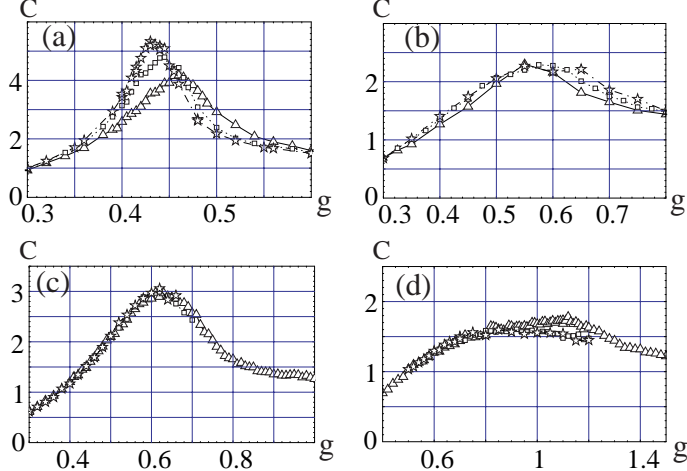


Figure 8: C vs g in the PD-2 and PD-3 models for $N = 8(\blacktriangle)$, $16(\blacksquare)$, $24(\star)$. (a) PD-2($\lambda = 1$), (b) PD-2($\lambda = 0$), (c) PD-3($\lambda = 1$), (d) PD-3($\lambda = 0$). The peak in C develops in (a) as N increases, whereas it does not in (b), (c) and (d). This indicates that the CDPT starts to appear between the two cases, (a) PD-2($\lambda = 1$) and (b) PD-2($\lambda = 0$).

We obtain a very interesting result, i.e., for the PD-2 system ($\alpha = 2$) with the *nonvanishing* spatial coupling $\lambda = 1$, there exists a second-order CDPT as in the PD-1 case, whereas in the PD-3 case ($\alpha = 3$) the peak in C does not develop as N increases, hence no signals of CDPT. Furthermore, careful study of the PD-2 case shows that the second-order CDPT *disappears* for *vanishing* spatial coupling $\lambda = 0$. Thus we conclude that the critical power is $\alpha_c = 2$ and the spatial coupling λ controls the existence of the CDPT. The above results will be confirmed by the study of the Polyakov line in the following subsection.

5.2 Polyakov lines

We have argued the possible CDPT by measuring the thermodynamic quantities like E and C . In order to study the CDPT in more details and further the nature of gauge dynamics in each phase, it is useful to calculate order parameters in gauge theory like Polyakov lines and Wilson loops.

First, let us introduce the Polyakov lines P_{x_\perp} for each spatial site $x_\perp \equiv (x_1, x_2)$ and study their

spatial correlations $f_P(x_\perp)$,

$$P_{x_\perp} = \prod_{x_0=1}^{N_0} U_{x_\perp, x_0, 0}, \quad x_\perp = (x_1, x_2),$$

$$f_P(x_\perp) = \langle \bar{P}_{x_\perp} P_0 \rangle. \quad (5.36)$$

Since the present model (3.18) contains no long-range interactions in the spatial directions, $f_P(x_\perp)$ is expected to supply a good order parameter to detect a possible CDPT. In the deconfinement phase, the fluctuations of U_{x_0} are small, which implies an order in $f_P(x_\perp)$, i.e., we expect $f_P(x_\perp) \neq 0$ as $x_\perp \rightarrow \text{large}$ in the deconfinement phase.

In Fig.9, we present $f_P(x_\perp)$ for the PD-1 and ED models. The PD-1 model of Fig.9(a) clearly exhibits an off-diagonal long-range order, i.e., $\lim_{x_\perp \rightarrow \infty} f_P(x_\perp) \neq 0$ for $g \geq 0.20$, whereas the ED model of Fig.9(b) *does not* for all g 's. To see this explicitly, we plot in Figs.9(c) and (d) the order parameter $p \equiv (f_P(x_\perp^{\text{MAX}}))^{1/2}$ for the PD-1 model, where $x_\perp^{\text{MAX}} \equiv N/\sqrt{2}$ is the distance at which f_P becomes minimum due to the periodic boundary condition. p of the PD-1 model($\lambda = 0$) starts to develop continuously from zero at $g = g_c \simeq 0.15$. The size dependence of p shows a typical behavior of a second-order phase transition. Thus the gauge dynamics of the PD-1 model is realized in the deconfinement phase for $g > g_c$, whereas it is in the confinement phase for $g < g_c$. In contrast, the ED model stays always in the confinement phase. These results including the value of g_c are in good agreement with those derived from the data of E and C given in Fig.5.

Let us turn to the PD-2 model with and without the spatial coupling. In Fig.10, we show the result of p for $\lambda = 1$ and $\lambda = 0$. We observe that the model with $\lambda = 1$ shows a typical behavior of the second-order phase transition as the system size is increased, whereas the case of $\lambda = 0$ does not. From this result and the observation of C in the previous subsection, we conclude that the CDPT exists in the PD-2 model ($\lambda = 1$) whereas it disappears in the PD-2 model ($\lambda = 0$).

In Fig.11 we present $f_P(x_\perp)$ of the PD-3 model. It is obvious that there is no long-range order in the PD-3 model both for $\lambda = 0, 1$ and only the confinement phase is realized for all g .

5.3 Wilson loops

Let us turn to study of the Wilson loops. For ordinary *pure and local* gauge systems, the Wilson loop $W[\mathcal{C}]$ along a closed loop \mathcal{C} on the lattice is a good order parameter to study the gauge dynamics; $W[\mathcal{C}]$ obeys the area law in the confinement phase and the perimeter law in the deconfinement phase;

$$W[\mathcal{C}] \equiv \langle \prod_{\mathcal{C}} U_{x\mu} \rangle \sim \begin{cases} \exp(-aS[\mathcal{C}]), & \text{area law,} \\ \exp(-a'L[\mathcal{C}]), & \text{perimeter law,} \end{cases} \quad (5.37)$$

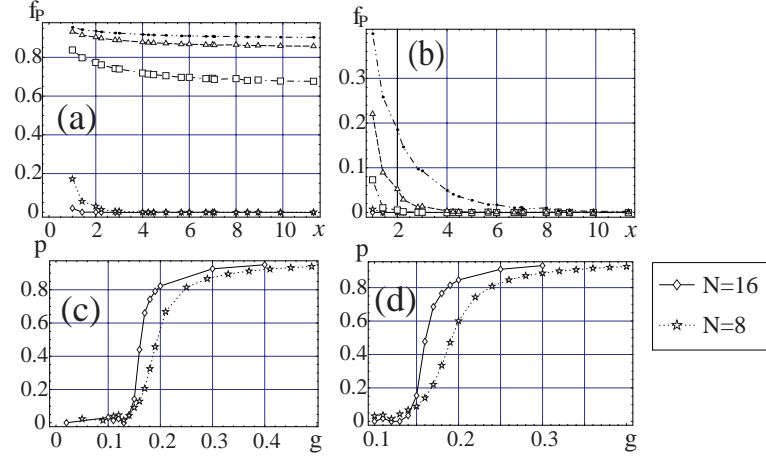


Figure 9: Correlations of Polyakov lines, $f_P(x_\perp)$, vs $|x_\perp|$. (a) PD-1 ($\lambda = 0$, $N=16$) with $g = 0.4, 0.3, 0.2, 0.1, 0.02$ from above. (b) ED ($\lambda = 0$, $N=16$) with $g = 2.5, 2.0, 1.5, 1.0, 0.5$ from above. In (c) and (d) the order parameter $p = (f_P(x_\perp^{\text{MAX}}))^{1/2}$ vs g is plotted for the PD-1 model; (c) PD-1 $\lambda = 0$ and (d) PD-1 $\lambda = 1$. They exhibit long-range orders for $g > g_c \simeq 0.15$ in the PD-1 model for both λ .

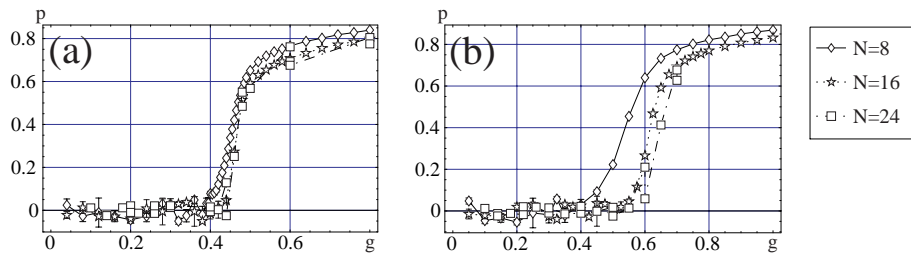


Figure 10: Off-diagonal long-range order of Polyakov lines, p vs $|x_\perp|$ for the PD-2 model with (a) $\lambda = 1$ and (b) $\lambda = 0$. In the $\lambda = 1$ case, p exhibits a steeper jump for larger N , whereas it does not in the $\lambda = 0$ case.

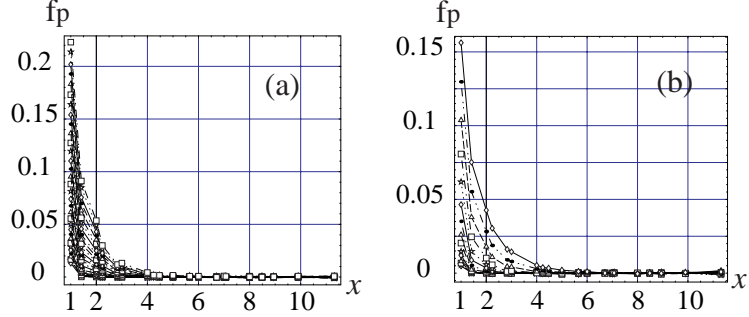


Figure 11: $f_P(x_\perp)$ vs g for the PD-3 model with $N = 16$; (a) $\lambda = 1$ for $g = 0.4 \sim 0.7$, (b) $\lambda = 0$ for $g = 0.56 \sim 0.78$. The upper curves have larger g 's. It is obvious that there is no long-range order in the PD-3 model regardless of the values of g and λ .

where $S[\mathcal{C}]$ is the minimum area of a surface, the boundary of which is \mathcal{C} , and a and a' are constants. For a (local) gauge theory containing matter fields of the fundamental charge, $W[\mathcal{C}]$ cannot be an order parameter because the matter fields generate the terms $\prod_{\mathcal{C}} U_{x\mu}$ with coefficients $\sim \exp(-bL[\mathcal{C}])$ in the effective action. However, in the present model (3.18), the nonlocal terms are restricted only along the temporal direction, so it is interesting to measure $W[\mathcal{C}]$ for the loops lying in the *spatial (1-2) plane*. If $W[\mathcal{C}]$ obeys the perimeter law, fluctuations of the spatial component of gauge field is small.

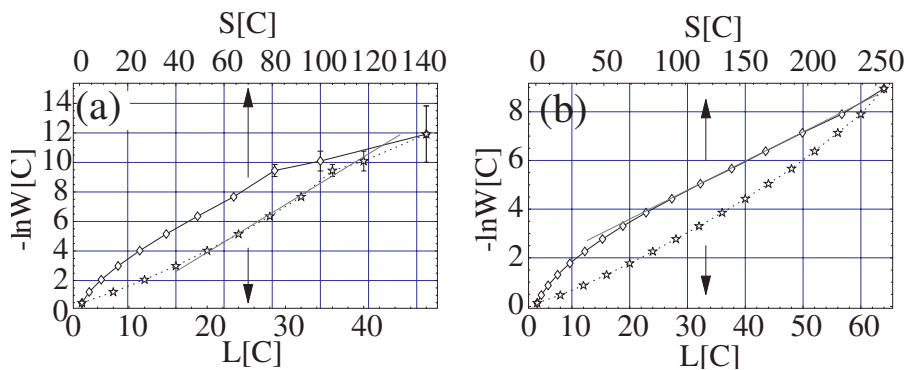


Figure 12: Wilson loops ($N = 32$) in the 1-2 plane at large g vs $L[\mathcal{C}]$ or $S[\mathcal{C}]$. (a) PD($\lambda = 1, g = 0.25$), (b) ED($\lambda = 1, g = 1.5$). The PD model seems to prefer the perimeter law, whereas the ED model prefers the area law.

In Fig.12, we plot $W[\mathcal{C}]$. For the PD-1 model in Fig.12(a), the data at $g = 0.25$ seem to prefer the perimeter law. For the ED model in Fig.12(b), the area law fits $W[\mathcal{C}]$ better than the perimeter law at $g = 1.5$; a considerably larger value than $g \simeq 1.0$ at the peak of C . This suggests that the area law holds in the ED model at all g . These observations are consistent with the previous results on the (non)existence of the CDPT. We conclude that the Wilson loops in the spatial plane can be used as an order parameter of gauge dynamics in the present model.

The result that the PD-1 case of the simplified model (3.18) exhibits the CDPT strongly suggests that the original model (3.16) of massless matter fields also has the deconfinement phase, because the isotropic distribution of the nonlocal gauge couplings in the original model should give the similar effect of suppression of fluctuations of $U_{x\mu}$ as those in the temporal direction in Eq.(3.18). This expectation is supported by the measurement of the spatial Wilson loop given above.

5.4 Instantons

It is well known in a 3D continuum space-time that instanton (monopole) configurations of $U(1)$ gauge field carry nontrivial topological numbers, and the instanton density serves as an index to express the disorderness of gauge field[11]. To see the details of gauge dynamics of the present model and to support the conclusions obtained in the previous sections, let us study instantons on the lattice. We employ the definition of the instanton density ρ_x at the site x in $U(1)$ lattice gauge theories by DeGrand and Toussaint [19]. We introduce the “vector potential” $\theta_{x\mu}$ as the exponent of $U_{x\mu} = \exp(i\theta_{x\mu})$ [$\theta_{x\mu} \in (-\pi, \pi)$]. Then, the magnetic flux $\Theta_{x,\mu\nu}$ penetrating plaquette $(x, x + \mu, x + \mu + \nu, x + \nu)$ is expressed as

$$\Theta_{x,\mu\nu} \equiv \theta_{x\mu} + \theta_{x+\mu,\nu} - \theta_{x+\nu,\mu} - \theta_{x\nu}, \quad (-4\pi < \Theta_{x,\mu\nu} < 4\pi). \quad (5.38)$$

We decompose $\Theta_{x,\mu\nu}$ into its *integer* part $2\pi n_{x,\mu\nu}$ ($n_{x,\mu\nu}$ is an integer) and the remaining part $\tilde{\Theta}_{x,\mu\nu} \equiv \Theta_{x,\mu\nu} \pmod{2\pi}$ uniquely,

$$\Theta_{x,\mu\nu} = 2\pi n_{x,\mu\nu} + \tilde{\Theta}_{x,\mu\nu}, \quad (-\pi < \tilde{\Theta}_{x,\mu\nu} < \pi). \quad (5.39)$$

Physically speaking, $n_{x,\mu\nu}$ describes the Dirac string whereas $\tilde{\Theta}_{x,\mu\nu}$ describes the fluctuations around it. The quantized instanton charge ρ_x at the cube around the site $\tilde{x} = x + \frac{1}{2} + \frac{\hat{\alpha}}{2} + \frac{\hat{\beta}}{2}$ of the dual lattice is defined as

$$\begin{aligned} \rho_x &= -\frac{1}{2} \sum_{\mu,\nu,\rho} \epsilon_{\mu\nu\rho} (n_{x+\mu,\nu\rho} - n_{x,\nu\rho}) \\ &= \frac{1}{4\pi} \sum_{\mu,\nu,\rho} \epsilon_{\mu\nu\rho} (\tilde{\Theta}_{x+\mu,\nu\rho} - \tilde{\Theta}_{x,\nu\rho}), \end{aligned} \quad (5.40)$$

where $\epsilon_{\mu\nu\rho}$ is the complete antisymmetric tensor. ρ_x measures the total flux emanating from the monopole(instanton) sitting at \tilde{x} . Roughly speaking, ρ_x measures the strength of nonperturbative gauge fluctuations around \tilde{x} . For the *local* 3D U(1) compact lattice gauge theory without matter fields, the average density

$$\rho \equiv \frac{1}{V} \sum_x \langle |\rho_x| \rangle, \quad (5.41)$$

is known to behave as $\rho \propto \exp(-cg)$ (c is a constant) if the instanton action cg is large; The instanton gas stabilizes the confinement phase for all the gauge coupling[11].

In Fig.13 we present ρ as a function of g in the PD-1 and ED models. It decreases as g increases more rapidly in the PD-1 model than in the ED model. This difference in behavior is consistent with the result that the PD-1 model exhibits a second-order transition, while the ED model does not. The λ coupling enhances the rate of decrease in ρ as one expects since the spatial coupling enhances the ordered deconfinement phase. In the ED model with $\lambda = 1$, ρ is fitted by $\exp(-cg)$ in the dilute (large g) region, and the smooth increase for smaller g indicates a *crossover* from the *dilute* gas of instantons to the *dense* gas, just the behavior similar to the case of pure and local lattice gauge theory[11, 20].

In Ref.[10] we presented the figure (Fig.3) which is very similar to Fig.13. However, the former was plotted by using the definition $\rho \equiv V^{-1} \sum_x \langle (1 - \delta_{0,\rho_x}) \rangle$, the average of occupation number of instantons (1 for $\rho_x \neq 0$ and 0 for $\rho_x = 0$) per site instead of the instanton density of Eq.(5.41) itself. The curves in two figures are almost indistinguishable, because the configurations with $|\rho_x| \geq 2$ are rather rare.

In Fig.14 we present snapshots of ρ_x for the PD-1 model with $\lambda = 1$. Fig.14(a) is a dense gas whereas Fig.14(b) is a dilute gas. They are separated at $g_c \simeq 0.20$, the location of the peak of C for $N = 16$. In Fig.14(b), instantons mostly appear in dipole pairs at nearest-neighbor sites, $\rho_x = \pm 1, \rho_{x \pm \mu} = \mp 1$, while in Fig.14(a), they appear densely and it is hard to determine their partners. In both cases, the distributions ρ_x have no apparent anisotropies like column structures. However, the orientations of dipoles in Fig.14(b) are mostly ($\sim 92\%$) in the temporal direction as expected from the nonlocal interactions of Eq.(3.18).

Next, let us examine the difference of gauge dynamics in various cases of nonlocal interactions in detail. To this end, it is useful to measure new observables made out of gauge-field configurations; nonlocal instantons elongated in the temporal direction with the length $t = 2, 3, \dots, N - 1$. The density of these instantons is defined by

$$\rho_{x,t} \equiv \sum_{\tau=0}^{t-1} \rho_{x+\tau\hat{0}},$$

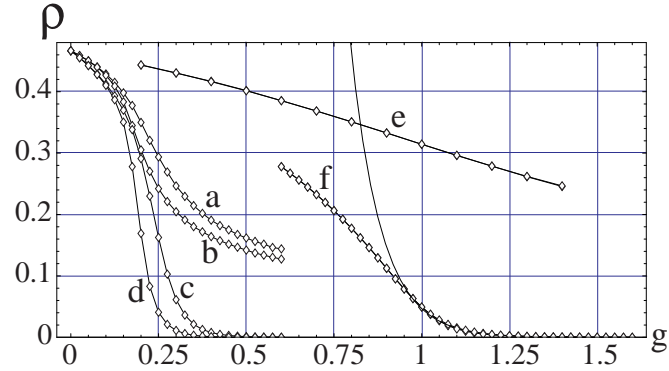


Figure 13: Average instanton density ρ vs g . (a)PD-1($\lambda = 0$, $N = 8$), (b)PD-1($\lambda = 0$, $N = 16$), (c)PD-1($\lambda = 1$, $N = 8$), (d)PD-1($\lambda = 1$, $N = 16$), (e)ED($\lambda = 0$, $N = 8, 16$), (f)ED($\lambda = 1$, $N = 8, 16$). The solid curve is $\propto \exp(-cg)$ and fits (f) at large g .

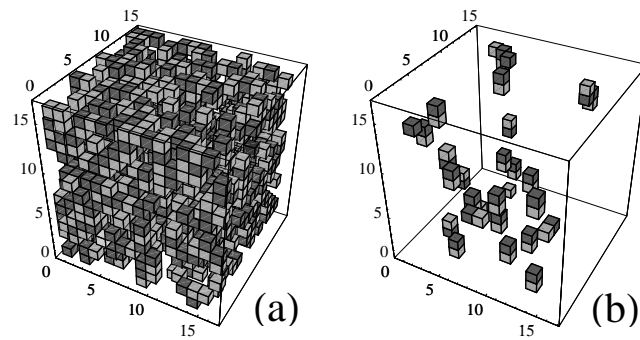


Figure 14: Snapshots of instanton configuration ρ_x on the 16^3 lattice for (a) PD-1($\lambda = 1$, $g = 0.15$), and (b) PD-1($\lambda = 1$, $g = 0.30$). The light cubes denote $\rho_x = 1$ and the dark cubes $\rho_x = -1$.

$$\rho_t \equiv \langle \rho_{x,t} \rangle. \quad (5.42)$$

In Fig.15 we plot ρ_t vs g for various cases of the exponent α and λ .

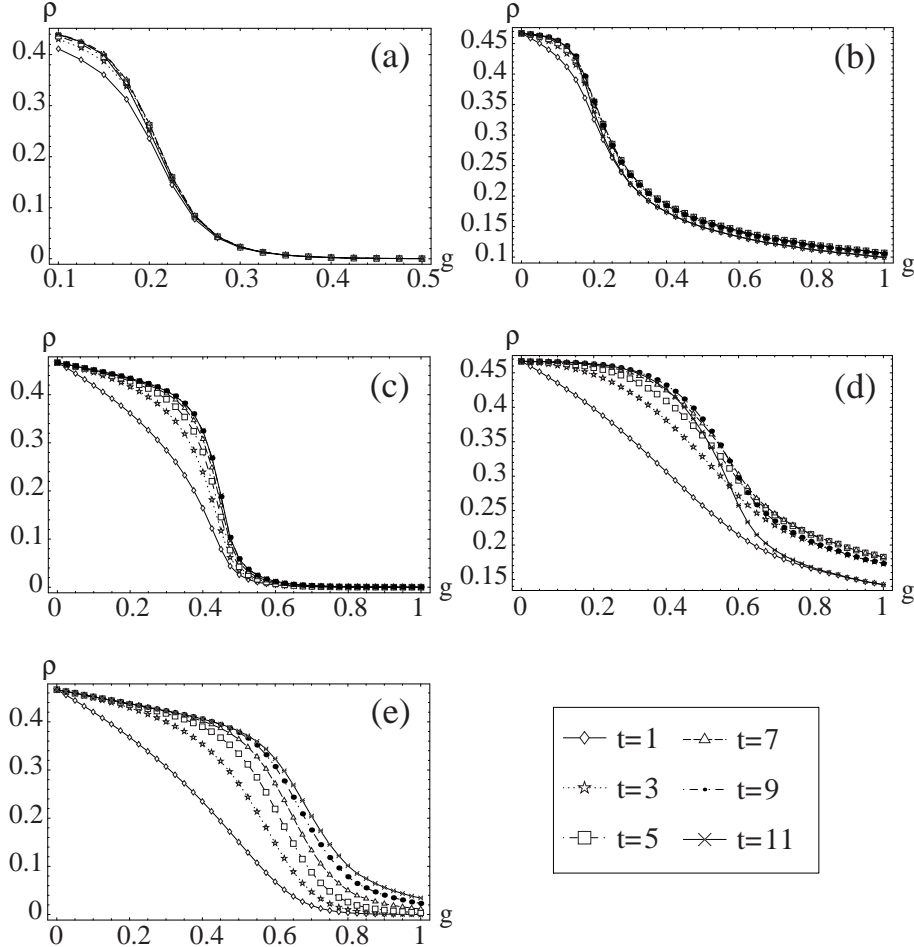


Figure 15: Density of nonlocal instantons ρ_t vs g for $N = 12$. (a) PD-1($\lambda = 1$), (b) PD-1($\lambda = 0$), (c) PD-2($\lambda = 1$), (d) PD-2($\lambda = 0$), (e) PD-3($\lambda = 1$). ρ_t at a fixed g increases as t increases.

We notice that ρ_t 's in Fig.15(a,b,c) behave quite differently from ρ_t 's in Fig.15(d,e). For the former cases, all the curves of ρ_t with different t 's decrease similarly as g increases [except for $t = 1$ in (c)], whereas for the latter cases, each ρ_t decreases in a different manner. The present nonlocal instanton density ρ_t is capable to distinguish the cases (a,b,c) exhibiting a CDPT and the cases (d,e) without transition (cross over) through its t dependence. This is consistent with our common understanding that the second-order phase transition is a collective phenomenon at which wild fluctuations of all the variables in the system in the disordered phase start to be reduced coherently

and also scale-invariantly near the transition point.

6 Effective Models at Large g and $\lambda = 0$

In this section, we study a 1D XY spin model for the *spatial* gauge variables U_{xi} and also a 2D XY spin model for the *temporal* ones U_{x0} , both of which are regarded as effective models for the present nonlocal model at large g and $\lambda = 0$ obtained by a simple reduction of the dynamical degrees of freedom. Two models are complementary each other and study of them helps us to understand the properties of the present nonlocal gauge model studied by the numerical simulations in section 5. In particular, these models are capable to explain the existence of the deconfinement (ordered) phase in the PD-1 model at large g and the nonexistence of it in the other PD and ED models with $\lambda = 0$.

6.1 The 1D XY model with spatial variables U_{xi}

Let us imagine the situation in which fluctuations of the temporal gauge fields U_{x0} are small so that one may replace $U_{x0} = \exp(i\theta_{x0})$ by its average as follows;

$$U_{x0} \rightarrow u \quad (0 < u < 1). \quad (6.43)$$

This is expected for sufficiently large g . Furthermore we put $\lambda = 0$, i.e., there are no direct interactions among spatial gauge variables $U_{xi} = \exp(i\theta_{xi})$. Then the system is decoupled to 1D subsystems defined at each spatial link $(x, x + i)$. The subsystem at $(x, x + i)$ is described by the U(1) angles $\theta_j (\equiv \theta_{xi})$ (we write $j = x_0$ and suppress the suffix x_1, x_2, i). Its energy takes the form of a 1D XY spin model with nonlocal interactions with couplings c_τ . The partition functions of the subsystem and the total system are given as follows;

$$Z_{1\text{DXY}} = \prod_{j=1}^N \int_{-\pi}^{\pi} \frac{d\theta_j}{2\pi} \exp \left[g \sum_{j=1}^N \sum_{\tau=1}^N u^{2\tau} c_\tau \cos(\theta_{j+\tau} - \theta_j) \right],$$

$$Z_{\mathcal{T}}(g : \text{large}, \lambda = 0) \simeq (Z_{1\text{DXY}})^{2N^2}. \quad (6.44)$$

To study the correlation function $\langle \exp[i(\theta_r - \theta_0)] \rangle$, we make the harmonic approximation for large g ; (i) expand the cosine term up to the quadratic term, (ii) extend the range of θ_j to $(-\infty, \infty)$ and (iii) neglect topologically nontrivial configurations. We expect that the third approximation in the above is justified by the *long-range ferromagnetic* interactions in Eq.(6.44). Then we have

$$Z_{1\text{DXY}} \simeq \prod_{j=1}^N \int_{-\infty}^{\infty} \frac{d\theta_j}{2\pi} \exp \left[-\frac{g}{2} \sum_{j=1}^N \sum_{\tau=1}^N u^{2\tau} c_\tau (\theta_{j+\tau} - \theta_j)^2 \right]$$

$$\begin{aligned}
& \propto \prod_{k=1}^N \int_{-\infty}^{\infty} d\tilde{\theta}_k \exp \left[-\sum_{k=1}^N G_k \tilde{\theta}_k^2 \right], \\
G_k &= g \sum_{\tau} u^{2\tau} c_{\tau} [1 - \cos(k\tau)], \\
f(r) &\equiv \langle \exp[i(\theta_r - \theta_0)] \rangle = \exp[-\frac{1}{2} \langle (\theta_r - \theta_0)^2 \rangle] \\
&= \exp[-\sum_k G^{-1}(k) (1 - \cos(kr))], \tag{6.45}
\end{aligned}$$

where $\tilde{\theta}_k$ is the Fourier-transformed variable of θ_j . For the standard local coupling $c_{\tau} = \delta_{\tau 1}$, the k -sum in the exponent of $f(r)$ gives $\int dk \cos(kr)/k^2 \sim r$, which implies $f(r) \simeq \exp[-(gu^2)^{-1}r] \rightarrow 0$ as $r \rightarrow \infty$ due to the severe infrared fluctuations. For the nonlocal cases we have

$$\begin{aligned}
f(r) &\simeq \exp \left[-\sum_k \frac{1 - \cos(kr)}{g \sum_{\tau} u^{2\tau} c_{\tau} \tau^2 k^2} \right] \simeq \exp(-Mr), \\
M &= \frac{1}{g \sum_{\tau} u^{2\tau} c_{\tau} \tau^2} \rightarrow \begin{cases} 0, & \text{PD-1} \\ \frac{1-u^2}{gu^2}, & \text{PD-2} \\ -\frac{1}{g \ln(1-u^2)}, & \text{PD-3} \\ \frac{(1-h)^3}{gh(1-h+3h^2-h^3)}, \quad (h = u^2 e^{-1}) & \text{ED} \end{cases}. \tag{6.46}
\end{aligned}$$

Namely, the order in the correlation function survives as $N \rightarrow \infty$ for the PD-1 case if $u \neq 0$, whereas the order is destroyed in the other cases even for $u \neq 0$. This result is just consistent with the numerical results for specific heat and the Polyakov lines studied in section 5. For $\lambda = 0$ case, the ordered-deconfinement phase is realized only in the PD-1 model at large g .

6.2 The 2D XY model with temporal variables U_{x0}

The discussion in the previous subsection is supported by considering another effective model that focuses on the dynamics of the temporal gauge field U_{x0} . To obtain it, we first replace the spatial gauge field U_{xi} by its average,

$$U_{xi} \rightarrow v \quad (0 < v < 1). \tag{6.47}$$

This replacement is supported for the PD-1 model by the result of the 1D XY model (6.46) in the previous subsection. Then we fix the gauge to the temporal gauge by setting $U_{x0} = 1$ except for $x_0 = N$ because of the periodic boundary condition. By keeping only the terms in the energy involving $U_{x_{\perp},N0}$, we have

$$\begin{aligned}
U_{x_{\perp},N} &\equiv \exp(i\varphi_{x_{\perp}}), \\
Z_{2\text{DXY}} &= \prod_{x_{\perp}} \int_{-\pi}^{\pi} \frac{d\varphi_{x_{\perp}}}{2\pi} \exp(A_{2\text{DXY}}),
\end{aligned}$$

$$A_{2\text{DXY}} = gv^2 \sum_{x_\perp} \sum_{i=1,2} \sum_{\tau=1} c_\tau \cos(\varphi_{x_\perp+i} - \varphi_{x_\perp}). \quad (6.48)$$

This is just the standard 2D XY spin model having the *nearest-neighbor couplings* among the XY spins $\exp(i\varphi_{x_\perp})$. Here the XY spin correlation function corresponds to the correlation function of the Polyakov lines studied in section 5,

$$\langle \cos(\varphi_{x_\perp} - \varphi_{0_\perp}) \rangle = f_P(x_\perp). \quad (6.49)$$

The spin stiffness in the effective 2D XY model is given as

$$gv^2 Q_1 \rightarrow \begin{cases} \infty, & \text{PD - 1} \\ \frac{gv^2 \pi^2}{6}, & \text{PD - 2} \\ \frac{gv^2 \pi^4}{90}, & \text{PD - 3} \\ \frac{gv^2}{e-1}, & \text{ED} \end{cases}. \quad (6.50)$$

It is well known that the 2D XY model with finite spin stiffness has no long-range order, although the Kosterlitz-Thouless transition is possible. Only in the PD-1 case, the spin stiffness diverges for finite v and the model may have the order $\langle U_{x_\perp, N0} \rangle \neq 0$. This result (6.50) supports the procedure (6.43) for the 1D XY model in the previous subsection for the PD-1 case. On the other hand, Eq.(6.46) supports the replacement (6.47) as we mentioned before. Thus studies of these two XY models give us the conclusion that only the PD-1 model at large g has the ordered (Coulomb) phase for the $\lambda = 0$ case.

Studies of the two effective XY models in this section predict that the cases of PD-2, PD-3 and ED with $\lambda = 0$ have no Coulomb phase, as it was verified by the previous numerical calculations. Inclusion of λ term, however, generates direct interactions between the spatial variables U_{xi} . For small λ , U_{xi} 's ($i = 1, 2$) can be integrated out perturbatively in powers of λ . The obtained effective model contains nonlocal and multi-body interactions of φ_{x_\perp} 's which prefer the ferromagnetic order of φ_{x_\perp} . Therefore the effective model for $\lambda \sim 1$ may *not* belong to the same universality class of the 2DXY model with local interactions. Then the above result does *not* contradict the numerical result in the previous section, which shows the deconfinement phase exists in the PD-2 model with $\lambda = 1$.

7 Conclusion

In this paper, we studied the nonlocal compact U(1) gauge theory on the 3D lattice, which “simulates” gauge models coupled with massless/massive matter fields. The main contributions of the present paper may be the following two points: (i) MC simulations are feasible within reasonable computer time even for 3D lattice gauge theories with nonlocal interactions along one direction,

and (ii) the measurements of E, C , Polyakov lines, Wilson loops, and local and nonlocal instantons give rise to clear and consistent results on the phase structure of the system; In particular, they distinguish the cases of ND($\lambda = 1, 0$), PD-1($\lambda = 1, 0$), PD-2($\lambda = 1$) with a CDPT from the other cases of PD-2($\lambda = 0$), PD-3, ED without CDPT in a definitive manner.

As explained in Sect.2.4, the results obtained in this paper are quite important for studies of the strongly-correlated electron systems like the high- T_c cuprates, the fractional quantum Hall effect, quantum spin models, etc. For example, in the t-J model of high- T_c superconductivity, by using the hopping expansion of holons and spinons at finite T with the continuous imaginary time, we derived an effective gauge theory, which is highly nonlocal in the temporal direction. The obtained effective theory has a similar action as Eq.(3.18) with $c_\tau = \text{constant}$ and $g \propto n$ where n is the density of matter fields(holons and spinons)[4]. This corresponds to the ND model. Although the above effective gauge model is obtained for the system at finite T , we expect that a similar gauge model appears as an effective model at $T = 0$. The result that the ND model has a CDPT strongly suggests that the t-J model has the corresponding phase transition into the deconfinement phase, which is nothing but the charge-spin separated phase.

In the deconfinement phase, all the three variables $U_{x\mu}$ ($\mu = 0, 1, 2$) are stable, having small fluctuations. The stability of the Lagrange multiplier U_{x0} means that the constraint (2.9) is *not* respected by the holons and spinons, the low-energy excitations of the system, whereas the stability of U_{xi} indicates that the gauge interaction between the holons and spinons can be treated perturbatively. Therefore, quasi-particles in the CSS state are the holons, spinons and weakly interacting gauge bosons[4]. Of course, in order to present a definite “proof” of the CSS, it is necessary to investigate a gauge system with full isotropic nonlocal interaction, because the integration over holons and spinons generates nonlocal interactions not only in the temporal direction but also in the spatial directions and their combinations.

Another interesting model related with the present one is the U(1) Higgs model coupled with the nonlocal gauge field. At present, it is believed that there is *no phase transition* in the 3D U(1) gauge-Higgs model with the ordinary local action if the Higgs field has the fundamental charge and its radial fluctuations are suppressed[21]. However, the situation may be changed by nonlocal gauge interactions. The existence of the deconfinement phase in the present nonlocal gauge system without Higgs fields suggests that all the three phases, i.e., the confinement, Coulomb and Higgs phases, may be realized in the 3D nonlocal gauge model with a local coupling to a Higgs field. The deconfinement phase of the present model corresponds to the Coulomb phase. This problem is closely related with “doped holes” in the algebraic spin liquid which may be realized in certain antiferromagnetic spin models and materials in the spatial 2D lattice. We shall report on these problems in a separate

publication[22].

Acknowledgement

One of the authors (K.S.) thanks the members of Department of Physics, Kanazawa University for their hospitality delivered to him during his stay.

References

- [1] G.Baskaran and P.W.Anderson, Phys.Rev.B37(1988)580;
A.Nakamura and T.Matsui, Phys.Rev.B37(1988)7940;
D.P. Arovas and A. Auerbach, Phys.Rev.B38(1988)316;
L.B.Ioffe and A.L.Larkin, Phys.Rev.B39(1989)8988;
I.Ichinose and T.Matsui, Phys.Rev.B45(1992)9976.
- [2] R.B.Laughlin, Phys.Rev.Lett.50(1983)1395;
J.K.Jain, Phy.Rev.Lett.63(1989)199.
- [3] P.W.Anderson, Phy.Rev.Lett.64(1990)1839.
- [4] For the quantum Hall states, see I.Ichinose and T.Matsui, Phys.Rev.B68(2003)085322 and the references cited therein. For the high-temperature superconductivity, see I.Ichinose and T.Matsui, Nucl.Phys.B394(1993)281; Phys.Rev. B51(1995)11860; I.Ichinose and T.Matsui, and M.Onoda, Phys.Rev.B64(2001)104516.
- [5] C.Nayak, Phys.Rev.Lett.85, 178(2000);
I.Ichinose and T.Matsui, Phys.Rev.Lett.86, 942(2001). See also the last reference of Ref.[4].
- [6] E.Fradkin and S.H.Shenker, Phys.Rev.D19(1979)3682.
- [7] Y.Iwasaki, K.Kanaya, S.Sakai, and T.Yoshie, Phys.Rev.Lett.69(1992)21.
- [8] J.B.Kogut and C.G.Strouthos, Phys.Rev.D67, 034504
(2003) and references cited there in.
- [9] The appearance of QED_3 is argued explicitly for the antiferromagnetic Heisenberg model in I. Affleck and J.B. Marston, Phys.Rev.B37(1988)3774, and for the slave-fermion t-J model in the last reference of Ref.[1].
- [10] A part of the results obtained in this paper has already been reported in G.Arakawa, I.Ichinose, T.Matsui, and K.Sakakibara, Phys.Rev.Lett.94 (2005) 211601.
- [11] A.M.Polyakov, Nucl.Phys.B120(1977)429.
- [12] H.Kleinert, F.S.Nogueira, and A.Sudbø, Phys.Rev.Lett.88(2002)232001;
Nucl.Phys.B666(2003)361;
F.S.Nogueira and H.Kleinert, cond-mat/0501022.

- [13] I.F.Herbut and B.H.Seradjeh, Phys.Rev.Lett.91(2003)171601;
I.F.Herbut, B.H.Seradjeh, S.Sachdev, and G.Murthy, Phys.Rev.B68(2003)195110.
- [14] S. Kragset, A. Sudbø, and F. S. Nogueira, Phys. Rev. Lett. 92 (2004)186403;
K. Børkje, S. Kragset, and A. Sudbø, Phys. Rev. B 71 (2005) 085112.
- [15] I.Ya.Aref'eva and S.I.Azakov, Nucl.Phys.B162(1980)298.
- [16] S.Takashima, I.Ichinose, and T.Matsui, cond-mat/0504193.
- [17] A.Jevicki, Phys.Rev.D20(1979)3331.
- [18] See, for example, J.M.Thijssen, “*Computational Physics*” (Cambridge University Press, 1999).
- [19] T.A.DeGrand and D.Toussaint, Phys.Rev.D22(1980)2478.
- [20] R.J.Wensley and J.D.Stack, Phys.Rev.Lett.63(1989)1764.
- [21] See, for example, M.N.Chernodub, E.-M.Ilgenfritz and A.Schiller, Phys.Lett.B547(2002)269;
S.Wenzel, E.Bittner, W.Janke, A.M.J.Schakel, and A.Schiller, cond-mat/0503599.
- [22] S.Takashima, K.Sakakibara, I.Ichinose, and T.Matsui, paper in preparation.